The Role of Islands in Sea Ice Transport Through Nares Strait

Brandon P. Montemuro[1*] and Georgy E. Manucharyan[1]

[1]School of Oceanography, University of Washington, Seattle, WA, USA.

*Corresponding author(s). E-mail(s): bpm5026@uw.edu; Contributing authors: gmanuch@uw.edu;

Abstract

This paper is a non-peer reviewed preprint submitted to EarthArXiv and has been submitted for publication to Nature Communications for peer review. Subsequent versions of this manuscript may have slightly different content.

Keywords: Sea Ice, Nares Strait, Discrete Element Model

1 Abstract

Nares Strait is a major pathway from the Arctic Ocean and an important climate system component. Sea ice's granular nature is pertinent in such straits with small islands where floes propagate by fracturing upon collisions. Since climate models are relatively coarse and use continuous sea ice rheology, they only partially capture the complexities of floe interactions. We use a floe-scale model, SubZero, to explore the role of islands in sea ice transport through Nares Strait. We demonstrate that SubZero can reproduce the crucial observed sea ice characteristics, including the area transport and variance in area fluxes. We found that a size-dependent critical stress criterion was necessary to simulate the power-law exponent in this domain's floe size distribution. Conducting simulations with and without the islands, we demonstrate the effectiveness of floe-scale models in simulating sea ice dynamics in straits and emphasize small islands' crucial role in affecting overall transport.

2 Introduction

The loss of Arctic sea ice is a significant concern due to its effect on the global climate [1–3]. Over ten percent of the total Arctic sea ice volume is exported annually into the Atlantic Ocean through various pathways, including Fram, Nares, and Davis straits [4]. Understanding the dynamics of sea ice transport through straits is crucial for predicting the future loss of Arctic sea ice [5]. This study focuses on sea ice dynamics in Nares Strait, which is the second largest ice export pathway that connects the Arctic Ocean and the Labrador Sea [6], located between Greenland and the Canadian Archipelago (Figure 1a). The sea ice and freshwater transported via Nares Strait can have global implications as they affect deep water mass production in the Labrador Sea [7]. For example, the extensive upper layer freshening from extreme Arctic sea ice melt in 2023 may have been the cause of the deep convection shutdown [8]. With continuing global warming and weakening of sea ice in the Arctic Ocean, the sea ice export through Nares Strait has nearly tripled, increasing from 33,000 km^2 in 2000 to 87,000 km^2 in 2020 [5]. Despite its importance, modeling sea ice motion in Nares Strait is particularly challenging because of the pertinence of the granular behavior of sea ice, including floe fractures[9–11] and jamming[12–15], as well as the unpredictable formation and collapse of sea ice arches [14–17] (also called bridges) that lead to highly intermittent sea ice transport [18–20].

Sea ice propagation through Nares Strait is further complicated by the presence of small islands [21], ranging from about 1 to 30 km^2 in area(Figure 1. Despite their relatively small size (e.g., Hans Island is only about 1.3 km^2), sea ice frequently comes in contact with these islands, experiencing significant collision forces [22] that can result in dramatic floe fractures commonly observable from space (Figure 1c). On the one hand, islands could act as pinning points that temporarily prevent sea ice propagation. On the other hand, collisions with islands may significantly reduce floe sizes, which would result in

Fig. 1: Surface reflectance images of the Nares Strait

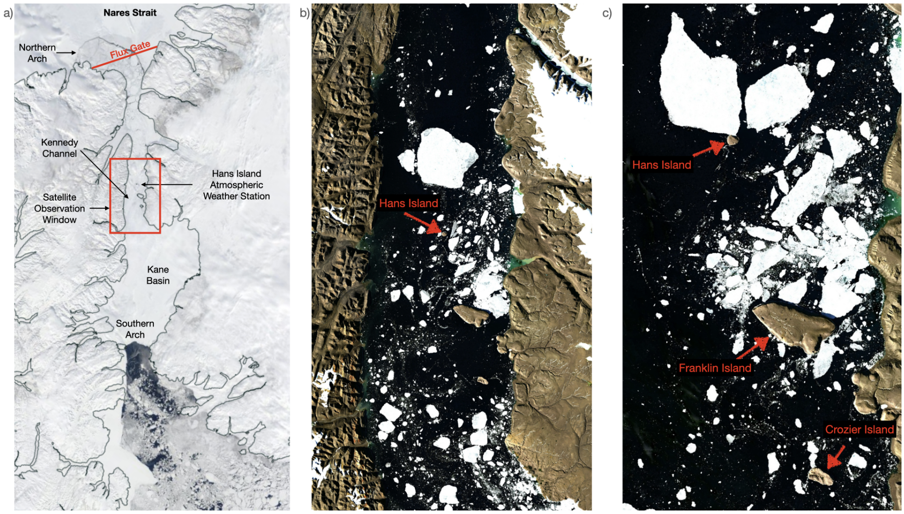

a) The Nares Strait showing conditions with both upper and lower sea ice arches formed (image taken NASA worldview 2023-05-04). Also indicated are the location of the Lincoln Sea flux gates (red line), Hans Island atmospheric weather station, and satellite observation window used to identify the floe size distributions (red rectangle). (b, c) Sea ice conditions after the breakup of arches as observed from Landsat-8 imagery on 2016-07-14 and 2016-07-16, respectively. Note the three major islands present in the Kennedy Channel section of Nares Strait. These visual observations of sea ice demonstrate large ice floes hitting Hans Island and fracturing into smaller pieces, some of which are then trapped by Franklin Island and temporarily kept from propagating through the channel.

smoother propagation of sea ice because granular media with smaller grains is known to be less prone to jamming[12]. Granular systems can jam when the forces holding them together are stronger than the forces trying to move them, such as when they are flowing through a narrow strait resulting in nearly zero motion [23–25]. Observations in different regions of the Arctic Ocean demonstrated that floe size distribution (FSD) of fragmented sea ice can be closely characterized by a power-law distribution, with exponents ranging from -3 to -1 depending on the region, season, and floe segmentation methodology [26–31]. While FSD may be playing a role in affecting the intermittency of sea ice transport, there are only very limited observational studies of it in the Nares Strait [32]. Thus, floe fractures and the effect of islands on FSD and the statistics of sea ice area transport remain poorly understood.

Climate models use continuous rheology [33], typically the elastic-viscous-plastic rheology [34] that does not explicitly simulate or take into account FSD in sea ice dynamics. Climate models are also very coarse and do not capture small islands, making it difficult to accurately represent the sea ice transport through Nares Strait, which is only a few tens of km wide at its narrowest point in the Kennedy Channel. Regional modeling studies explored aspects of sea ice motion in Nares Strait in both continuous and discrete element models (DEMs). The formation of arches has been simulated using a continuous

Fig. 2: The inputs used for running the simulation of the Nares Strait.

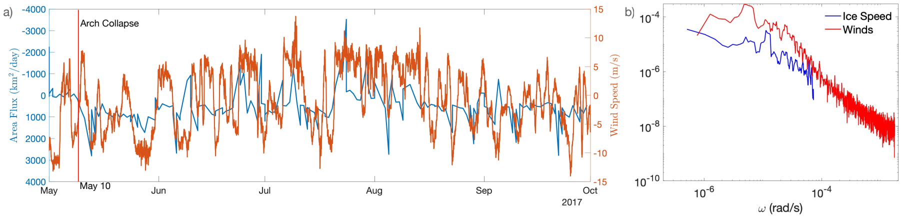

a) Observational sea ice area flux and wind speed aligned with the channel that forces the ice from May through Sept 2017 (Data taken from the atmospheric station on Hans Island and the southern Lincoln Sea flux gate). The observational area flux is positive when moving from the Lincoln Sea into the Nares Strait. The wind speed plotted here is aligned with the channel and is negative when moving in the direction from top to bottom. The simulation time used to force the model for this study is May 10 to May 20, 2017). b) The power spectral density of the observed ice and along channel wind velocities from 2017 dates shown. The power spectrum for winds is scaled by a factor of 0.02, which demonstrates where the ice velocity would be if it were in free drift. The gap in the power spectrum shows that energy is lost to ice-ice and ice-land interactions.

Maxwell elasto-brittle rheology [35] as well as with an elastic-viscous-plastic rheology [36], demonstrating the importance of arches (or bridges) in shutting down sea ice transport. However, such continuous models cannot be used to quantify the role of individual islands in the intermittent jamming behavior associated with propagation and fractures of clusters of floes. Sea ice DEMs were used to investigate jamming behavior in highly idealized constrictions [12], to explore the initial breakup events in complex coastal regions [37], and breakup up events with lead formation in parts of the Nares Strait [38]. However, the role of islands in the sporadic jamming, floe fractures, and propagation of sea ice through Nares Strait remains to be understood such that these processes could be parameterized in coarse-scale climate projection models. This study uses a unique sea ice DEM approach to explore the propagation of sea ice through Nares Strait shortly after the collapse of an arch, revealing the crucial role of floe collisions with small islands and coastal boundaries.

3 Results

To simulate the propagation of sea ice in a domain with realistic coastlines and forcing, we used a sea ice DEM, SubZero [39, 40], that represents ice floes as polygons that can change shapes and fracture into smaller floes in response to stresses from collisions and external forces. The sea ice is initialized with the observed concentration field and forced using observational winds recorded at the Hans Island atmospheric weather station (AWS) [41, 42] (see Methods). We first tuned the SubZero model to adequately simulate the observed FSD and area transport characteristics (see Sections 3.1 and 3.2). For model-data comparison, we reconstructed FSD from segmenting floes from satellite images in the Nares Strait (see Section 3.1), and used sea ice area fluxes obtained from existing Lincoln Sea flux gate measurements [43] at the entrance of the Nares

Fig. 3: The segmentation process of sea ice comparing the results from Terra satellite reflectance images (250m resolution) to Sentinel-2 satellite (17m resolution).

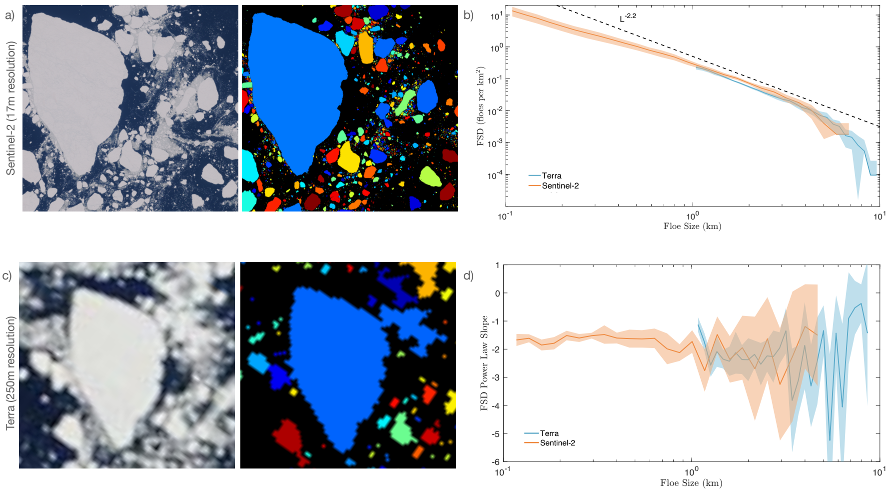

a) Input image and resulting segmented image from Sentinel-2. Image taken from SentinelHub for 2022-06-16 b)The FSD for both the Terra Satellite and Sentinel-2 comparing the observed distributions. c) Input image and resulting segmented image from Terra. Image taken from NASA worldview for 2022-06-16 d) The power-law slope fit comparing Terra and higher resolution Sentinel-2. The shading in parts (b) and (d) indicate the 95% confidence intervals.

Strait. Having demonstrated the model's adequacy in simulating the observed statistics of sea ice motion, we proceeded to quantify the role of the islands by comparing sea ice dynamics in simulations that either include or exclude the islands (see Section 3.3).

3.1 Observations of Transport and FSD in Nares Strait

Sea ice area transport through Nares Strait exhibits highly intermittent behavior, with some events being nearly three times stronger than its average transport and other times having almost no transport (Figure 2a). Right after an arch collapse (an example is shown for May 10, 2017 for which flux gate observations exist), there is a rapid transport of ice that is driven by strong southward winds, with an average sea ice transport of about 1000 km^2 per day over the course of the summer. However, the sea ice motion is not in free drift, as is clearly indicated by the discrepancy in the power spectra of the observed sea ice velocities and expected free-drift velocity based on the wind speeds, particularly at time scales longer than about a day (Figure 2b). Sea ice moving significantly slower than expected in free drift indicates that it looses energy and momentum not only due to ocean drag but also due to internal collisions and interactions with coastlines. The intermittency of sea ice transport is associated with a combination of strongly varying atmospheric winds and granular behavior of sea ice floes that leads to jamming. Note that for simulation purposes, we use the local Hans Island winds because they capture extreme wind events that are absent in the reanalysis data [41, 42].

Since there are no existing comprehensive observational studies on FSD in the Nares Strait, we developed a database of cloud-free optical images of sea ice taken from two satellites with very different resolutions (Terra at 250 m resolution and Sentinel-2 at 17 m). The sea ice images span the post-arch collapse period (from May to August) over a 14-year period for Terra and a seven-year period for Sentinel-2, where individual ice floes and their sizes were identified via the image segmentation algorithm[44] (see Figure 3 and Methods). FSDs estimated from both satellites are remarkably similar, following an approximate power-law distribution for a wide range of floe sizes (3b). The values of the best-fit power-law exponent range from about -1.7 to -2.8, with a mean of -2.2 across all images. This range of power laws falls within the range of existing FSD observations in other regions of the Arctic Ocean [26]. Note that here we present FSD as a function of floe size (square root of the area), but expressed in terms of floe area, the mean power-law exponent of -2.2 would be $\frac{1}{2}(-2.2) - 1 = -2.1$. Comparing it to the recent area-based FSD power-law estimate of [-2,-1.65] obtained using segmentation of very high-resolution (about 1 m) MEDEA images in the Canada Basin [30], there is also a good agreement, suggesting that floe fracturing processes in Nares Strait might be representative of many other regions of the Arctic Ocean.

3.2 Granular simulations of sea ice flow in Nares Strait

We conducted a process study to tune the model to the observational statistics from the Nares Strait described in section 3.1. We initialized the model with an ice concentration taken from post-collapse observations of a northern ice arch (Figure 4a) and forced the model with observed winds and prescribed ocean currents. The sea ice evolves from unrealistic initial conditions, with primarily uniform floe sizes, to a state with a wide range of floe sizes due to cascading floe fractures (Figure 4). During model tuning, nearly all model parameters remained the same as in the default model configuration [39] (see Table 1) but we have identified two key processes that most impacted the sea ice statistics: the strength of ocean currents that mainly affected the mean sea ice transport and the parameterization for the critical stress for floe fractures that mainly affected the FSD. Since there are no ocean observations coincident with flux gate and wind observations, we assumed a highly idealized ocean with constant currents moving down the channel. The ocean currents provide additional forcing to the sea ice and mainly affect the mean value of the sea ice area transport (see section 5.1.1). However, ocean currents did not impact the emerging power-law exponent of the FSD. To better match the model FSD to observations, we incorporated a scale-dependent parameterization for the critical fracture stress that was previously proposed in an observational study of sea ice fractures [10]. This parameterization assumes the critical stress required for floe fracture to be inversely proportional to the square root of

Fig. 4: The SubZero simulation showing the evolution of sea ice floes as they propagate through Nares Strait.

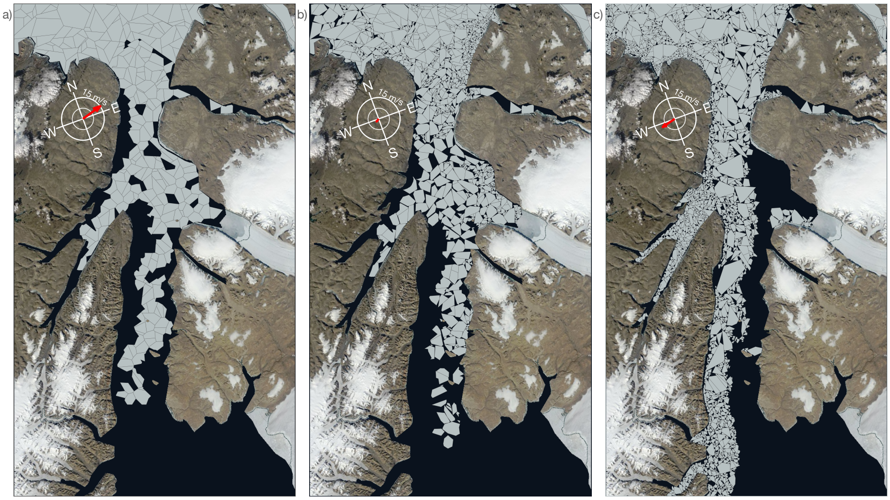

The three panels show the progression of the modeled state of ice floes as they evolve from a) unrealistic initial conditions where all floes have similar sizes to b) the state 1.5 days into the simulation after the winds have caused collisions and fractures that are particularly evident in the northern part of the channel, and c) the state 10 days into the simulation when the distribution of floe sizes have reached statistical equilibrium. The simulation resolves collisions of floes down to the minimum size of 1 km^2 and uses scale-dependent fracture criteria (see Methods).

its length scale, implying that larger floes could fracture under less stress (see Methods).

Upon only adjusting the strength of ocean currents and the floe fracture parameterization, quantitative metrics of the modeled FSDs, mean transport, and the transport variance reasonably agreed with observations. The sea ice area fluxes found in Nares Strait from flux-gate observations are of the order of $O(10^3)$ km^2/day [19] and the total ice area transport generally agree with the simulation (Figure 5a). A comparison of the observed distribution of the area fluxes over the breakup month (May 2017) to the modeled one also shows a good agreement, demonstrating that the intermittency of sea ice propagation has also been captured by the model. Simulated mean area fluxes are around 1000 km^2/day and the distribution has fat tails, with less frequent events having either very small transports or nearly triple the mean, which is similar to observations [13, 19]. As sea ice collisions lead to fracture events that generate smaller and smaller floes, these floes can then propagate through the relatively narrow strait (see Supplementary Video). After about five days of spin-up time, the modeled FSD equilibrates to power-law distribution with a best-fit exponent that is about -1.5 for the case of scale-independent critical stress and -2.2 for the scale-dependent (Figure 5c). Comparing the modeled and satellite-derived FSDs, we also find a remarkable agreement for simulations with scale-dependent critical stress (Figure 5d). Since the SubZero model

Fig. 5: Observed and SubZero modeled characteristics of sea ice floes and transport

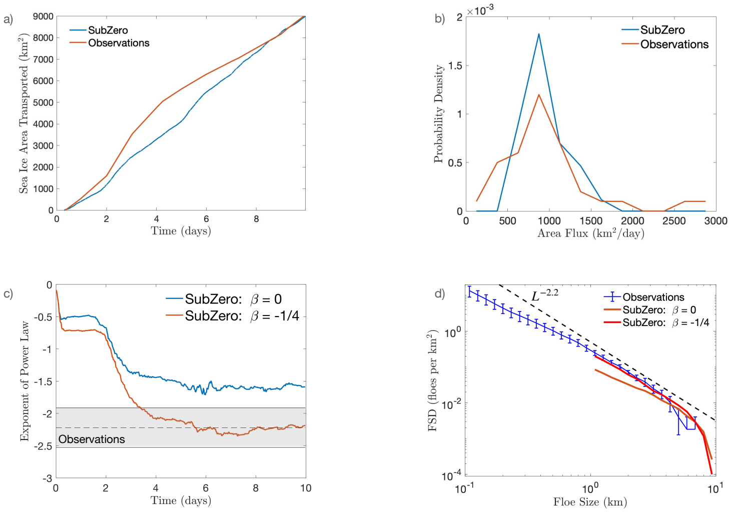

This figure shows a) the cumulative area transport for the SubZero simulation in comparison to the observed area transport over the same period we are simulation and b) the associated PDF for the fluxes with that run compared to observations of fluxes for the month following the collapse of the sea ice arch. c) Shows the time evolution of the instantaneous exponent of the power law over the run for a run with size-dependent fracture laws and one with size-independent fracture laws. d) The mean FSD for days four through ten for size-dependent fracture laws, the with size-independent fracture laws, and the mean observed FSD from the Nares Strait from Sentinel-2 imagery.

can reasonably reproduce the crucial observational characteristics of sea ice floes and transport, we proceed to quantify the role of the islands in sea ice transport.

3.3 Impact of islands on sea ice motion

To evaluate the influence of islands on ice transport, we use the tuned model conduct two types of simulations, with and without islands, and explore the response of sea ice to external forcing that we vary by using uniform winds of different strengths. At the start of both cases, with and without islands, the size of sea ice floes decreases through fracturing so they can more easily travel through the narrow strait (Supplementary Video 2). However, sea ice movement through these straits is only sometimes smooth, as large floes can become jammed in narrow areas, especially when islands are present. During a typical jamming event (Figure 6a), sea ice velocities near Hans Island are slowed to virtually zero, and the ice can not get past the island until stresses in that area build to the point of fracturing the ice floes. This jamming occurs when large floes cluster in narrow parts of the strait, and ice movement can only resume once some of these larger floes break into smaller pieces. However, when the islands are removed, it becomes much more challenging for the ice floes to jam,

Fig. 6: SubZero simulation snapshots showing the state of sea ice floes as they propagate through Nares Strait with and without islands

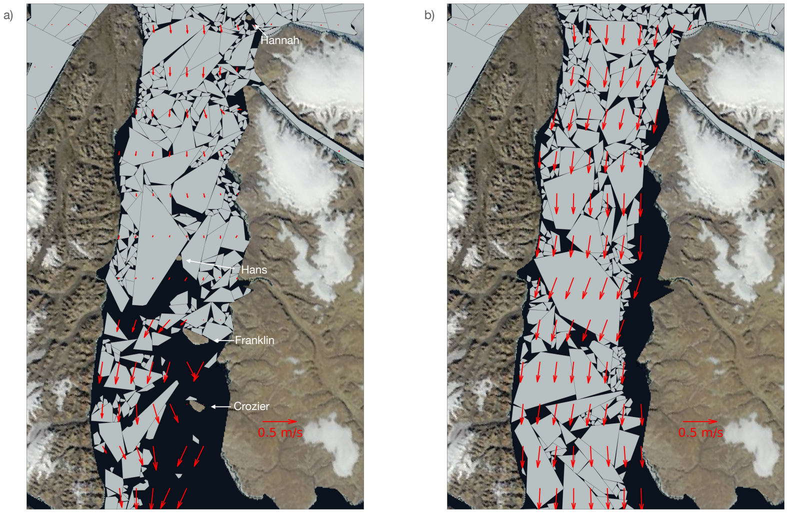

This figure compares simulations with a minimum floe size of 1 km^2 and floe size-dependent fractures for runs with and without the islands present. Wind speeds are constant at ten m/s, blowing from top to bottom. The arrows show equispaced spatially averaged instantaneous ice velocities. a) A snapshot of the model state five days into the run with islands. b) A snapshot of the model state five days into the run without islands.

and sea ice moves relatively smoothly (Figure 6b). Due to the island-induced jamming events, the average sea ice area flux through the strait is dramatically reduced, particularly in simulations with relatively low wind speeds (Figure 7). Excluding islands from the simulation nearly doubles the mean area flux and substantially reduces its variance because jamming becomes virtually negligent (see the lack of events with very weak area fluxes in Figure 7 a). As the external wind forcing increases, floe fractures become more frequent, reducing the potential for jamming to occur and making the mean sea ice transport in the simulations with and without the islands more similar (Figure 7 b).

During jamming events, when the ice gets pinned near islands and barely moves, forces from the islands and other coastal boundaries oppose the internal stress gradients that build up from local and remote atmospheric forcing. Domain-averaging collision and surface forces experienced by individual floes, we identified the contributions of the individual islands and other coastal boundaries to the momentum balance (Figure 8). During a major jamming event around day five (distribution of sea ice floes during this event is shown in Figure 6a), there is a clear spike in the force from Hans Island accompanied by a drop in the sea ice area flux (Figure 8a). There are many similar jamming events that do not lead to a complete blockage of sea ice but rather a substantial reduction in transport: for example, on Day 4, when Hans Island plays a big role, or close to Day 10, when Franklin Island is a key contributor

Fig. 7: The sea ice area fluxes and transport in Nares Strait from numerical simulations with and without islands.

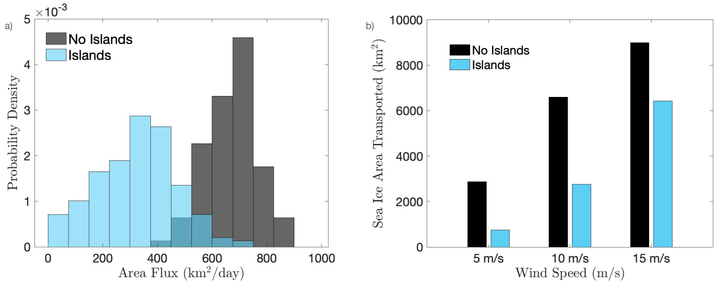

a) The distribution of sea ice area fluxes for the simulation using 10 m/s winds, with and without islands. b) The sea ice area transported over the total duration of the model simulation (about 10 days), computed at the channel location near Hans Island and plotted for different wind speeds. Note that direct comparisons of the fluxes with the tuning simulation that used realistic winds and optimized ocean currents (Figure 3.2) would lead to fluxes being biased low because the ocean in the sensitivity experiments shown here is taken to be stationary.

to the partial jamming (Figure 8a). During jamming, there is weak ocean drag as sea ice velocity is low and the ocean currents are set to zero in these simulations. As such, forces from islands/coasts oppose the external atmospheric forcing during jamming events. Considering the time-average breakdown of the momentum budget in the simulation with islands, combined forces from islands and coastlines become dominant, while the ocean drag provides a substantially smaller contribution because of the reduced sea ice velocity compared to the simulation without the islands (Figure 8b). The islands do not only provide direct collision forces but also lead to increased frictional forces at lateral coastal boundaries because the ice is pushed toward the channel's lateral boundaries as it propagates around the islands. Thus, the substantial weakening of sea ice transport when islands are included in simulations is due to the combined effect of having normal forces from ice floe collisions with islands and increased frictional forces at the coastal boundaries.

4 Discussion

This investigation emphasizes the important role of small islands in transporting sea ice through Nares Strait after the collapse of sea ice arches. Using a novel floe-scale sea ice model, SubZero, we conducted a process study to explain the observed characteristics of summer sea ice floes as they progressively break up due to collisions with each other and coastal boundaries. Such conditions where new ice is not being formed and floes do not weld but predominantly fracture due to collisions provided a natural laboratory to focus on the granular aspects of sea ice dynamics. We demonstrated that the model is capable of emulating the jamming of floes and the associated wide-tail distribution of sea ice area transport following the breakup of the sea ice arches. To accurately

Fig. 8: Domain-averaging collision and surface forces breakdown.

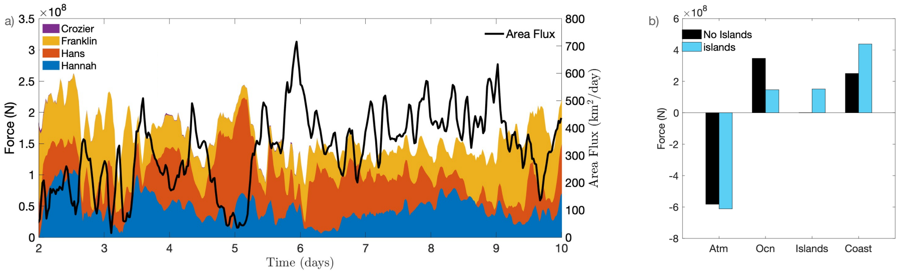

(a)The left y-axis shows the combined forces from islands over the final eight days of simulation, comparing with and without islands after a two-day spin-up for ten m/s winds. The upper boundary displays the total force of the islands at each instant, with colors indicating the portion from each individual island. The right y-axis measures the evolution of the sea ice area flux in Nares Strait over the final eight days of simulation with islands. (b) The time-average breakdown of the y-momentum budget in for the ten m/s winds simulations with and without islands. Mean values are taken over the last eight days of the run.

capture the observed FSD, the model implies that larger floes must fracture subject to lower stresses, following a size-dependent power-law distribution of critical stresses. By simplifying the model down to only collision-induced fractures and being able to reproduce the major aspects of the observed sea ice behavior, we demonstrated the significance of the granular-type sea ice dynamics. As sea ice floes propagate through the channel, the islands act as anchor points, causing frequent jamming events that significantly reduce long-term sea ice transport, especially during low to moderate wind conditions. In addition to intermittent jamming, the islands cause the coastal drag to increase by pushing the ice toward lateral coastal boundaries. This process study demonstrates the effectiveness of floe-scale modeling in accurately simulating sea ice dynamics in regions with islands and complex coastlines. The omission of islands, typical in climate models, could lead to significant overestimation of sea ice transport from the Arctic through the Nares Strait, contributing to uncertainties in predicting sea ice state in our evolving climate.

While our study focused on sea ice propagation after an arch collapse, understanding the formation of sea ice arches (or bridges) is also important because it leads to a total shutdown of ice export through Nares Strait. Frequent jamming events caused by the presence of islands may facilitate arch formation if they coincide with sufficiently low atmospheric temperatures to create new ice and weld existing floes together. It is necessary for climate models to accurately represent processes leading to the formation and collapse of arches, especially as the observed frequency of arch formation is changing with climate. Since climate models are typically too coarse to include small islands, it may be possible to use them in conjunction with regional floe-scale models such as SubZero to represent the effects of islands and complex coastal features in important regions like Nares Strait. Another way to improve continuous sea ice models used in climate simulations is to develop parameterizations based on floe-scale models. Finally, we emphasize the need for high-resolution sea ice observations to improve and fine-tune floe-scale models to better understand the granular nature of sea ice.

5 Methods

The installation of the Hans Island AWS was carried out collaboratively by a team comprising members from the United States, Canada, Denmark, and the United Kingdom in May 2008. Wind speed and direction data were made available beginning in September 2014 at 30-minute intervals through October 8, 2020, with some gaps in the data. [43] has sea ice flux data from 2016 to 2019. Because of the times when we had overlapping data sets, we chose to simulate the period from May 10, 2017, to May 20, 2017, when a sea ice arch collapsed. This paper utilized SubZero from [40] to explore the physical mechanisms leading to floe deformation, specifically fracturing.

5.1 Sensitivity Test

For our study, we randomly initiated the model with floes of approximately 2-3 times the maximum size observed in the region. These floes were of uniform thickness at 0.5m. More floes initialized north of the strait entrance (not shown in the figures) move in and push through the strait as the simulation progresses temporally. When this region with additional floes becomes empty, it is repopulated with new sea ice to keep a continuous supply entering the Nares Strait during these simulations. Floes are removed from the simulation once they have hit the bottom boundary of the simulation through the strait or drop below the designated minimum floe size. The same initial floe states were used for all ocean sensitivity tests and minimum floe size sensitivity tests. Additionally, all tests about sensitivity to the presence of islands are done with the same initial conditions that differ from the ocean/resolution tests. We used GPS coordinates to create a set of coastal boundaries, which are indestructible static floes in the model. Table 1 lists all other parameters set for this run.

This study presents an improved method for calculating a time-averaged stress history from Manucharyan et al. [39]. The previous SubZero model used an equally weighted mean to calculate the average stress over time. However, we have updated the model to use a weighting that gives higher importance to more recent stresses. Specifically, we are using an exponential decay approach to calculate the new average, as shown below:

$$\frac{d\sigma}{dt} = -\frac{1}{\tau}\left(\sigma - \sigma(t)\right) \tag{1}$$

Where τ is a weighting factor that controls the rate at which old stresses decrease exponentially with time. This new calculation provides a more accurate representation of the stress history over time and has the added benefit of reducing the space required in data structures. We no longer need to store the

N previous stresses, where N is the number of prior time steps being averaged over. Additionally, we utilize a scaling for fractures with the allowable stresses scaling like $l^{-1/2}$ [10], where l is a length scale, which makes large floes weaker and more susceptible to fracturing. Weaker large-scale floes were selected since large floes have a higher probability of defects within the ice.

5.1.1 Ocean Sensitivity Test

Ocean speeds within the Nares Strait, especially within the Kennedy Channel, are very strong and vary based on season, year, and ice coverage. At a minimum floe size resolution of one square kilometer, we perform a sensitivity test to determine the impacts of the underlying ocean currents on model outputs and the appropriate ocean speed for this specific model run since we do not have observations for the time of this study. Table 1 presents the model parameters used in the simulation. The wind data from May 10, 2017, to May 20, 2017, are sourced from the AWS on Hans Island, and the ocean is assumed to be pushing in the direction of the channel at velocities of 0.3 m/s and 0.4 m/s, moving from the Arctic to Kane Basin. We then use the sea ice area fluxes obtained from the Lincoln Sea flux gate measurements to validate and determine the appropriate ocean velocity. The SubZero code was modified to track the area flux of ice as it passes the flux gate line indicated in Figure 1a. Supplementary Figure 1 in the supplementary material show the model output sensitivity to the ocean currents on values such as the total area transport. As ocean velocities increase, the area fluxes tend to trend towards higher flux rates, as illustrated in the supplementary figures. The study shows that to match the observed area flux and transport at the one square kilometer resolution, we need to use an ocean speed of 0.3 m/s.

5.1.2 Resolution Test

We ran multiple resolution tests to determine the model sensitivity to the minimum floe size kept for simulations. The two floe minimum floe sizes used in this study are 1 km^2 and 10 km^2. The other model parameters used in the simulation are the same as presented in Table 1 from other studies. The winds here are still those from May 10, 2017, to May 20, 2017, and the ocean is assumed to be pushing in the direction of the channel at a velocity of 0.3 m/s based upon the results from section 5.1.1, moving from the Arctic to Kane Basin. Again, we compare this to sea ice area fluxes obtained from the Lincoln Sea flux gate measurements.

The study found that the size of ice floes can affect the movement of sea ice through narrow straits. As the size of sea ice floes decreases, they can more easily travel through the narrow strait. However, sea ice movement through these straits is not always smooth, as large floes can become jammed in narrow areas. This jamming occurs when large floes cluster in narrow parts of the strait, and ice movement can only resume once some of these larger floes break into smaller pieces. The study found that coarser resolutions are more susceptible to jamming, as larger floes can become stuck, while finer resolutions floes remain capable of breaking to relieve the stress. The study estimated sea ice area fluxes in Nares Strait using the idealized simulation. The sea ice area fluxes in Nares Strait from flux-gate observations are around 10^3 km^2/day (Moore et al., 2021) and are of the same order for flux rates. However, the coarser simulations tended to underpredict the total amount of ice area transported throughout the run, as illustrated in the supplementary figure 2. The study also found that the floe size distribution (FSD) takes the form of a single power-law distribution with an exponent close to -2. The FSD is free to equilibrate to a different power-law exponent depending on the forcing and floe interaction and fracture laws. As the sea ice breaks into smaller floes, they can propagate through the relatively narrow strait. The breaking of floes depends on the fracture criteria, and the floe fractures lead to intermittent but large fluxes of sea ice area and transported mass. Supplementary figure 2 in the supplementary material present the floe size distributions associated with different runs, indicating good consensus between the medium and fine-scale simulations of a decade of floe sizes when compared against observations.

5.1.3 Wind Speed Variation Test

We assess the impact of islands on the simulation by utilizing SubZero to simulate runs that start at full sea ice coverage and idealized forcing conditions. To accomplish this, we employ the same initial conditions across all test cases except for the islands within the Kennedy Channel. We ran a suite of tests in which the islands were and were not present within the Kennedy Channel section of Nares Strait over a range of wind speeds to assess the impact of the islands when the channel is completely covered in ice. These floes were of uniform thickness at 0.5m and covered north of Kane Basin up to the Lincoln Sea. Full ice coverage represents the period when the lower arch is breaking up and the ice is starting to leave the Kennedy Channel. These exact initial floe states were used for all tests. The minimum floe size is one square kilometer, and the ocean speed is set to 0 m/s. For this study, we set the model to track the movement of sea ice past the vertical location of Hans Island in the center of the Kennedy Channel. All other parameters are the same as in 1. The wind speeds for these runs are 5 m/s, 10 m/s, and 15 m/s, blowing down the channel from top to bottom and 0 m/s in the cross-channel direction. We used GPS coordinates to create a set of coastal boundaries and islands that are indestructible static floes as before. However, for half of the runs, the indestructible static floes in the middle of the channel are now allowed to move and break like normal floes, which removes the islands from the simulation.

5.2 Optical Imagery Observations

We segmented and retrieved the areas of sea ice floes using optical satellite imagery from acquired in the Nares Strait between from May to August over a 14-year period for Modis and a seven-year period for Sentinel-2. Clear days after the ice breakup within the Nares Strait were selected to ensure individual fragments could be identified. Images were collected between May and August 2016-2023, and the images used for calculating the observational with image dates indicated in the file names have been made publicly available (see data availability). Floe identification was achieved through Denton's image segmentation algorithm [44], which utilizes a modified "restricted growing" approach first described by Tsatsoulis et al. [45] and furthered by Denton et al. [30]. The image was preprocessed into a binary image and manually classified into ice (floes) and water (background) based on a grayscale threshold, followed by an iterative erosion-expansion scheme to produce a segmented image. Any floes cut off by the image borders or located on land were removed. Here we use the cumulative form, FSD(x), where FSD is the fractional number of floes larger than x. The segmented images are utilized to construct an FSD using a modified method from Rothrock and Thorndike [11]. Unlike previous studies, the FSD is normalized by the identified floes' total area rather than the image's total area. This adjustment accounts for the area covered by the land mask and ensures that the curves lie on each other. The remaining segmented image was used to retrieve floe areas and construct an FSD, which was employed to validate the SubZero model. Results are characterized by a single power law with (linear least-squares fit) slope alpha for the regime of floe areas covered by Modis imagery for comparison between the two satellites. These values are listed in Table 2.

Table 1: A list of key parameters used in the SubZero model Nares Strait simulation, including their default numerical values, a brief description, and the processes that use these parameters.

Parameter	Description	Process
$E = 5 \times 10^7$ Pa	Young's Modulus	Floe Interactions
$G = \frac{E}{2(1+\nu)}$	Shear Modulus	
$\nu = 0.3$	Poisson's ratio	
$\mu = 0.25$	Coefficient of Friction	
N_{Frac}=150	Time steps between fracturing	Floe Fractures
$N_{Pieces} = 3$	Number of pieces for fracturing	
$P^* = 5 \times 10^4$ N m^{-1}	Floe strength-to-thickness ratio	
$\rho_i = 920$ kg m^{-3}	Density of ice	Floe mass and moment of inertia
$\rho_a = 1.2$ kg m^{-3}	Density of air	Surface stresses
$\rho_o = 1027$ kg m^{-3}	Density of ocean	
$Cd_{atm} = 10^{-3}$	Atmosphere-ice drag coefficient	
$Cd_{ocn} = 3 \times 10^{-3}$	Ocean-ice drag coefficient	
$N_{MC} = 100$	Number of sample points for Monte Carlo integration over floe surface	
$\Delta t = 5$ s	Integration time step	Time stepping
$N_b = 25$	Number of floes creating the boundary with islands	Floe state
$N_b = 21$	Number of floes creating the boundary without islands	

Table 2: A list of dates and least squares fit for power law slope for days with both Modis and Sentinel-2 imagery.

Date	Modis alpha-value	Sentinel-2 alpha-value
2016-07-14	-1.9	-1.7
2019-06-08	-2.8	-2.8
2019-07-25	-1.8	-2
2022-05-13	-2.3	-1.75
2022-06-15	-2.5	-2.6
2022-07-25	-2.3	-2.5
2023-07-14	-2.2	-2.2

Acknowledgments. B.P.M and G.E.M gratefully acknowledge support from the Office of Naval Research (ONR) grant N00014-19-1-2421. The authors are extremely grateful for the valuable contributions made by our undergraduate researchers, Yuna Liu and Camille Viviani, to this research. The authors also highly appreciate the insightful discussions at the online workshop "Modeling the Granular Nature of Sea Ice" organized by the School of Oceanography, University of Washington as part of the ONR MURI project N00014-19-1-2421.

Data Availability

The most up to date SubZero code [?] is provided at the public GitHub repository https://github.com/SeaIce-Math/SubZero. SubZero v1.0.5 [46] associated with this publication and test cases shown above can be found on Zenodo https://doi.org/10.5281/zenodo.13730444. The images used for observational FSD calculations can be found on Zenodohttps://doi.org/10.5281/

zenodo.13770011. The author would like to thank the Scottish Association for Marine Sciences for access to the Hans Island automatic weather station data (https://dataservices.sams.ac.uk/aws/).

References

[1] Chiang, J.C., Bitz, C.M.: Influence of high latitude ice cover on the marine intertropical convergence zone. *Climate Dynamics* **25**(5), 477–496 (2005)

[2] Curry, J.A., Schramm, J.L., Ebert, E.E.: Sea ice-albedo climate feedback mechanism. *Journal of Climate* **8**(2), 240–247 (1995)

[3] Deser, C., Walsh, J.E., Timlin, M.S.: Arctic sea ice variability in the context of recent atmospheric circulation trends. *Journal of Climate* **13**(3), 617–633 (2000)

[4] Spreen, G., de Steur, L., Divine, D., Gerland, S., Hansen, E., Kwok, R.: Arctic sea ice volume export through fram strait from 1992 to 2014. *Journal of Geophysical Research: Oceans* **125**(6), 2019–016039 (2020)

[5] Babb, D.G., Galley, R.J., Howell, S.E., Landy, J.C., Stroeve, J.C., Barber, D.G.: Increasing multiyear sea ice loss in the beaufort sea: A new export pathway for the diminishing multiyear ice cover of the arctic ocean. *Geophysical Research Letters* **49**(9), 2021–097595 (2022)

[6] Howell, S., Babb, D., Landy, J., Moore, G., Montpetit, B., Brady, M.: A comparison of arctic ocean sea ice export between nares strait and the canadian arctic archipelago. *Journal of Geophysical Research: Oceans*, 2023–019687 (2023)

[7] Zhang, J., Weijer, W., Steele, M., Cheng, W., Verma, T., Veneziani, M.: Labrador sea freshening linked to beaufort gyre freshwater release. *Nature communications* **12**(1), 1229 (2021)

[8] Yashayaev, I.: Intensification and shutdown of deep convection in the labrador sea were caused by changes in atmospheric and freshwater dynamics. *Communications Earth & Environment* **5**(1), 156 (2024)

[9] Weiss, J.: Fracture and fragmentation of ice: a fractal analysis of scale invariance. *Engineering Fracture Mechanics* **68**(17-18), 1975–2012 (2001)

[10] Weiss, J., Schulson, E.M.: Coulombic faulting from the grain scale to the geophysical scale: lessons from ice. *Journal of Physics D: Applied Physics* **42**(21), 214017 (2009)

[11] Rothrock, D.A., Thorndike, A.S.: Measuring the sea ice floe size distribution. *Journal of Geophysical Research: Oceans* **89**(C4), 6477–6486

(1984)

[12] Damsgaard, A., Adcroft, A., Sergienko, O.: Application of discrete element methods to approximate sea ice dynamics. *Journal of Advances in Modeling Earth Systems* **10**(9), 2228–2244 (2018)

[13] Kwok, R., Toudal Pedersen, L., Gudmandsen, P., Pang, S.: Large sea ice outflow into the nares strait in 2007. *Geophysical Research Letters* **37**(3) (2010)

[14] Rallabandi, B., Zheng, Z., Winton, M., Stone, H.A.: Formation of sea ice bridges in narrow straits in response to wind and water stresses. *Journal of Geophysical Research: Oceans* **122**(7), 5588–5610 (2017)

[15] Rallabandi, B., Zheng, Z., Winton, M., Stone, H.A.: Wind-driven formation of ice bridges in straits. *Physical review letters* **118**(12), 128701 (2017)

[16] Moore, G., Howell, S., Ballinger, T., McNeil, K., Brady, M.: Contribution of ice dynamics along nares strait to the stability of ice arches. Preprint at https://doi.org/10.21203/rs.3.rs-3976407/v1 (2024)

[17] Kirillov, S., Babb, D., Komarov, A., Dmitrenko, I., Ehn, J., Worden, E., Candlish, L., Rysgaard, S., Barber, D.: On the physical settings of ice bridge formation in nares strait. *Journal of Geophysical Research: Oceans* **126**(8), 2021–017331 (2021)

[18] Moore, G., Howell, S., Brady, M.: Evolving relationship of nares strait ice arches on sea ice along the strait and the north water, the arctic's most productive polynya. *Scientific Reports* **13**(1), 9809 (2023)

[19] Moore, G., Howell, S., Brady, M., Xu, X., McNeil, K.: Anomalous collapses of nares strait ice arches leads to enhanced export of arctic sea ice. *Nature communications* **12**(1), 1 (2021)

[20] Detlef, H., Reilly, B., Jennings, A., Mørk Jensen, M., O'Regan, M., Glasius, M., Olsen, J., Jakobsson, M., Pearce, C.: Holocene sea-ice dynamics in petermann fjord in relation to ice tongue stability and nares strait ice arch formation. *The Cryosphere* **15**(9), 4357–4380 (2021)

[21] Joshy, K., Moore, G., McNeil, K.: Transient wind-driven polynyas within nares strait. Preprint at 10.22541/essoar.171501009.93805419/v1 (2024)

[22] Danielewicz, B., Metge, M., Dunwoody, A.: On estimating large scale ice forces from deceleration of ice floes. *The Seventh International Conference on Port and Ocean Engineering under Arctic Conditions*, 537–546 (1983)

[23] Cates, M., Wittmer, J., Bouchaud, J.-P., Claudin, P.: Jamming, force chains, and fragile matter. *Physical review letters* **81**(9), 1841 (1998)

[24] To, K., Lai, P.-Y., Pak, H.: Jamming of granular flow in a two-dimensional hopper. *Physical review letters* **86**(1), 71 (2001)

[25] Zuriguel, I.: Invited review: Clogging of granular materials in bottlenecks. *Papers in physics* **6**(2), 0–0 (2014)

[26] Stern, H.L., Schweiger, A.J., Zhang, J., Steele, M.: On reconciling disparate studies of the sea-ice floe size distribution. *Elem Sci Anth* **6**, 49 (2018)

[27] Stern, H.L., Schweiger, A.J., Stark, M., Zhang, J., Steele, M., Hwang, B.: Seasonal evolution of the sea-ice floe size distribution in the beaufort and chukchi seas. *Elem Sci Anth* **6**, 48 (2018)

[28] Hwang, B., Wilkinson, J., Maksym, T., Graber, H.C., Schweiger, A., Horvat, C., Perovich, D.K., Arntsen, A.E., Stanton, T.P., Ren, J., *et al.*: Winter-to-summer transition of arctic sea ice breakup and floe size distribution in the beaufort sea. *Elem Sci Anth* **5**, 40 (2017)

[29] Zhang, Q., Hughes, N.: Ice floe segmentation and floe size distribution in airborne and high-resolution optical satellite images: towards an automated labelling deep learning approach. *The Cryosphere* **17**(12), 5519–5537 (2023)

[30] Denton, A.A., Timmermans, M.-L.: Characterizing the sea-ice floe size distribution in the canada basin from high-resolution optical satellite imagery. *The Cryosphere* **16**(5), 1563–1578 (2022)

[31] Buckley, E.M., Cañuelas, L., Timmermans, M.-L., Wilhelmus, M.M.: Seasonal evolution of the sea ice floe size distribution from two decades of modis data. *EGUsphere* **2024**, 1–16 (2024)

[32] Horvat, C.: Floes, the marginal ice zone and coupled wave-sea-ice feedbacks. *Philosophical Transactions of the Royal Society A* **380**(2235), 20210252 (2022)

[33] Keen, A., Blockley, E., Bailey, D.A., Boldingh Debernard, J., Bushuk, M., Delhaye, S., Docquier, D., Feltham, D., Massonnet, F., O'Farrell, S., *et al.*: An inter-comparison of the mass budget of the arctic sea ice in cmip6 models. *The Cryosphere* **15**(2), 951–982 (2021)

[34] Hunke, E.C., Dukowicz, J.K.: An elastic–viscous–plastic model for sea ice dynamics. *Journal of physical oceanography* **27**(9), 1849–1867 (1997)

[35] Dansereau, V., Weiss, J., Saramito, P., Lattes, P., Coche, E.: Ice bridges and ridges in the maxwell-eb sea ice rheology. *The Cryosphere* **11**(5), 2033–2058 (2017)

[36] Rasmussen, T.A., Kliem, N., Kaas, E.: Modelling the sea ice in the nares strait. *Ocean Modelling* **35**(3), 161–172 (2010)

[37] Åström, J., Robertsen, F., Haapala, J., Polojärvi, A., Uiboupin, R., Maljutenko, I.: A large-scale high-resolution numerical model for sea-ice fragmentation dynamics. *The Cryosphere* **18**(5), 2429–2442 (2024)

[38] West, B., O'Connor, D., Parno, M., Krackow, M., Polashenski, C.: Bonded discrete element simulations of sea ice with non-local failure: Applications to nares strait. *Journal of Advances in Modeling Earth Systems* **14**(6), 2021–002614 (2022)

[39] Manucharyan, G.E., Montemuro, B.P.: Subzero: A sea ice model with an explicit representation of the floe life cycle. *Journal of Advances in Modeling Earth Systems*, 2022–003247 (2022)

[40] Montemuro, B.P., Manucharyan, G.E.: Subzero: a discrete element sea ice model that simulates floes as evolving concave polygons. *Journal of Open Source Software* **8**(88), 5039 (2023)

[41] Moore, G.: Impact of model resolution on the representation of the wind field along nares strait. *Scientific Reports* **11**(1), 13271 (2021)

[42] Moore, G., Imrit, A.: Impact of resolution on the representation of the mean and extreme winds along nares strait. *Journal of Geophysical Research: Atmospheres* **127**(19), 2022–037443 (2022)

[43] Moore, G.: Nares Strait Ice Area Flux. https://doi.org/10.5683/SP2/WRGX0K. https://doi.org/10.5683/SP2/WRGX0K

[44] Denton, A.A.: Sea-Ice Floe Segmentation. https://doi.org/10.5281/zenodo.6336109

[45] Tsatsoulis, C., Kwok, R., Soh, L.-K., Tsatsoulis, C., Holt, B.: Identifying ice floes and computing ice floe distributions in sar images. *Analysis of SAR Data of the Polar Oceans: Recent Advances*, 9–34 (1998)

[46] Montemuro, B.P., Manucharyan, G.E.: SubZero: a Discrete Element Sea Ice Model that Simulates Floes as Evolving Concave Polygons. https://doi.org/10.5281/zenodo.13730444